COBEM 2023 27TH INTERNATIONAL CONGRESS OF MECHANICAL ENGINEERING

ABCM Brazilian Society of Mechanical Sciences and Engineering
27th ABCM International Congress of Mechanical Engineering
December 04-08, 2023, Florianópolis-SC, Brazil

COB-2023-1249
ANALYSIS OF A NITI BLADE-TYPE SPRING WITH SUPERELASTIC EFFECT ACCORDING TO MANUFACTURING PROCESSES

Igor Jordan Guilherme de Sena
Academic Unit of Mechanic Engineering Federal University of Campina Grande
igor.jordan@estudante.ufcg.edu.br
Richard Senko
Academic Unit of Production Engineering Federal University of Campina Grande
richard.senko@ufcg.edu.br
Antônio Almeida Silva
Academic Unit of Mechanic Engineering Federal University of Campina Grande
Antonio.almeida@ufcg.edu.br
Vinicius da Silva Almeida
Academic Unit of Mechanic Engineering Federal University of Campina Grande
Viniciusalmeida.eng.mecanico@gmail.com

Abstract.
The application of smart materials in rotating systems as vibration attenuators is well-established due to their vibration reduction capabilities. One of the most common types of smart materials used is Shape Memory Alloys (SMA), which exhibit property changes in response to temperature (shape memory effect - SME) or mechanical stress (superelasticity - SE). The objective of this research is to compare and analyze the manufacturing of superelastic NiTi blade-type springs, considering different heat treatment methods, mechanical forming processes, and fabrication techniques (shape setting), with the aim of achieving a balance in properties. By optimizing these factors, it was possible to obtain a final austenitic temperature of 14.88°C, an increased hysteresis damping of 78.44%, and a rupture strength of 1285.23 MPa. These results demonstrate the high potential of the springs in passive vibration reduction in rotating systems.

Keywords: *Shape memory alloys, superelasticity, rotating systems.*

1. INTRODUCTION

The extensive application and studies involving smart materials are due to their ability to alter physical properties when subjected to external stimuli. Among these materials are piezoelectrics, electro and magneto-rheological fluids, and shape memory alloys (SMAs) (GANDHI, THOMPSON, 1992), with the latter being the focus of this study. SMAs are smart materials that, after being deformed, have the ability to recover their original shape when subjected to temperature or mechanical stress variations.

This ability is due to the material's crystalline structure, which exhibits different effects depending on the martensitic and austenitic phases, such as shape memory effect (SME) and superelasticity (SE). When the material is fully in the martensitic phase, changes occur in the crystalline structure when subjected to temperature and stress variations. Superelasticity occurs above the austenite finish temperature (Af) when the mechanical stress is applied to the material, resulting in an elastic deformation of up to 8% in NiTi alloys and inducing a phase transformation to martensite.

According to the literature, these alloy behaviors are influenced by factors such as material composition, cold work, heat treatments, among others (LAGOUDAS, 2008; OTSUKA and WAYMAN, 1999; PATOOR, LAGOUDAS, et al., 2006). Due to these characteristics, the applications of SMAs encompass various areas such as dentistry, medicine, and engineering, with the latter focusing on reducing undesirable vibrations in rotating systems.

This research aims to analyze and compare the manufacturing methods, heat treatments, and mechanical forming of superelastic NiTi blade-type springs with the study conducted by Almeida (2020), who utilized water quenching as a cooling method for the samples. By employing different methods, it is expected to achieve improved damping capacity and mechanical strength, as well as a final austenite temperature close to room temperature, enabling the activation of the superelastic effect without the requirement of external heating. This makes it feasible to passively reduce vibrations in rotating systems.

2. METHODOLOGY

The methodology of this research followed the steps of the flowchart presented in Figure 1.

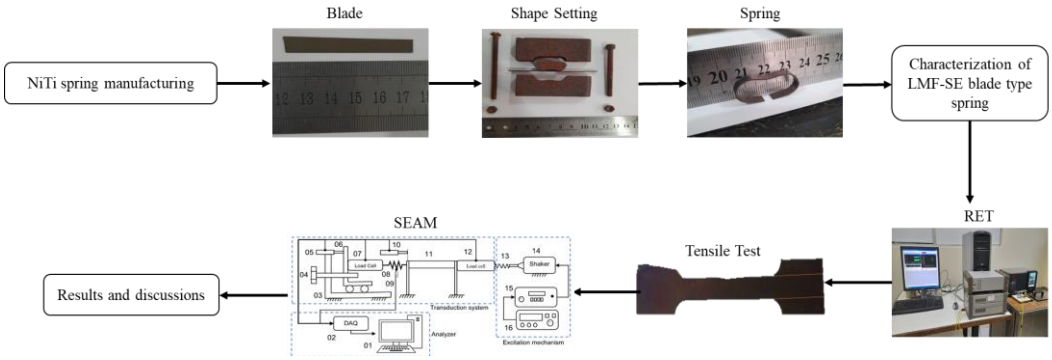

Figure 1. Research flowchart. Source: Prepared by the author.

2.1 Manufacturing of LMF-SE blade type spring

For the manufacturing of C-shaped LMF-SE blade-type springs as proposed by Senko (2018), Figure 2, the initial step involved the use of an electroerosion machine to cut the NiTi sheet with a nickel weight percentage of 55.8%, resulting in samples with a length of 64 mm, width of 5 mm, and thickness of 0.52 mm.

Figure 2. C-shaped blade spring. Source: Adapted from SENKO, SILVA, et al., (2020).

With the samples in these dimensions, a heat treatment (HT) was performed for homogenization and stress relief (SOUZA, 2015), at a temperature of 450°C for 10 minutes, as recommended by the manufacturer. Subsequently, natural convection cooling was carried out to achieve an austenite finish (Af) temperature close to ambient and high mechanical strength, based on studies conducted by HEIDARI, KADKHODAEI, et al., (2016). To obtain the C-shaped form (Figure 3), shape setting was performed using a carbon steel mold consisting of three pieces connected by screws, as shown in Figure 3(A). After inserting the sample into the mold, a HT was carried out at a temperature of 500°C for 30 minutes, followed by natural convection cooling. These shape setting parameters are suggested by RAO, SRINIVASA, et al., (2015). At the end of the shape setting process, the C-shaped blade springs obtained the form shown in Figure 3(B).

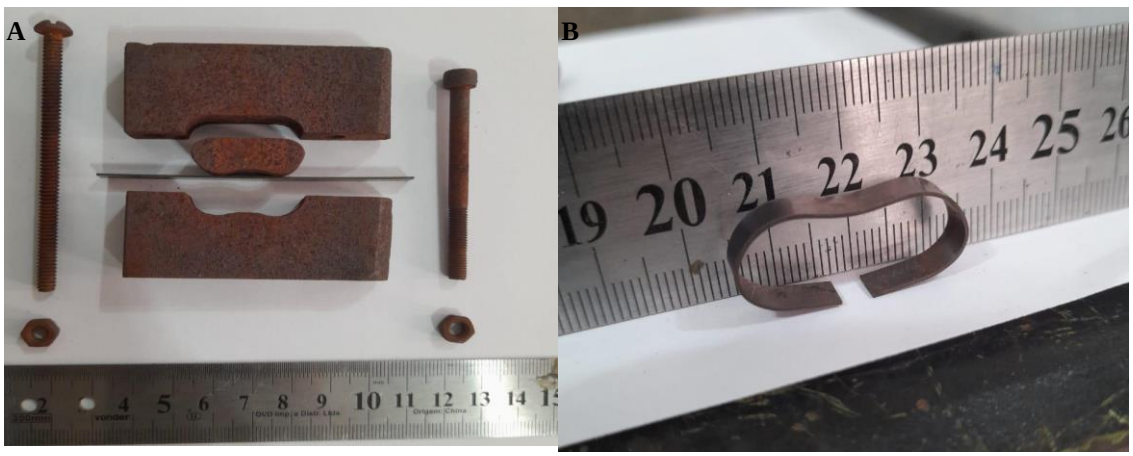

Figure 3. (A) Carbon steel mold, (B) C-shaped blade. Source: Prepared by the author.

2.2 Characterization of LMF-SE blade type spring

2.2.1 Characterization of transformation temperatures

To determine the phase transformation temperature values of the C-shaped LMF-SE blade springs, the electrical resistance variation with temperature (RET) technique was employed, as depicted in Figure 3. This technique involves controlled temperature variation of the sample while simultaneously monitoring the temperature and electrical resistance, enabling the acquisition of the experimental curve of electrical resistance versus temperature (DOS REIS, 2010).

For the test setup, as depicted in Figure 4, a power source (1) is required to provide fixed current (0.574 A) and potential difference to the sample, which is fixed on a base (3). The sample is immersed in a thermal bath (2) whose temperature (T) is controlled using a device (4). Temperature measurements are obtained through a type K thermocouple attached to the sample and transmitted to the data acquisition system (5), along with the potential difference (voltage) from the power source. The acquired data is then sent to a computer (6).

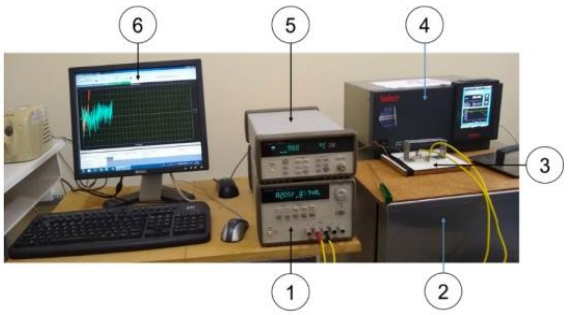

Figure 4 - RET. Source: Almeida (2020).

2.2.2 Mechanical characterization

To determine the yield strengths and verify the mechanical properties of the spring, a mechanical characterization was performed following the standard procedure for tensile testing of wires in NiTi alloys, ASTM F2516.26200 (2014). The test specimens, as shown in Figure 5, were produced by electroerosion cutting of LMF alloy sheets.

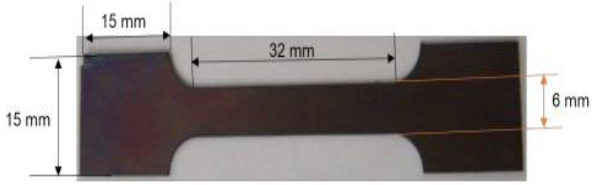

Figure 5. Tensile test specimen. Source: Almeida (2020)

This procedure was also carried out by Almeida (2020), where the samples were subjected to loading up to 6% deformation, followed by unloading to a stress lower than 7 MPa, and then loaded until fracture. This was done using an Instron® 5582 tensile testing machine equipped with a video extensometer (AVE) at room temperature (approximately 22 ºC) and a deformation rate of 0.04 mm/min. According to the standard, the following results are to be observed: Upper plateau strength (UPS): Stress at 3% deformation during sample loading; Lower plateau strength (LPS): Stress at 2.5% deformation during sample unloading; Residual Elongation (ELr): Difference between the initial deformation and the deformation at the moment the test reaches 7 MPa during unloading; Uniform Elongation: Elongation determined at the maximum force sustained by the sample before necking, cracking, or both. Additionally, the austenitic and martensitic elastic moduli and transformation stresses are also obtained.

2.2.3 Material damping characterization

Finally, to determine the damping factor of the material, experiments were conducted using the System for Material Damping Estimation (SEAM), as depicted in Figure 6, as presented by DOS REIS, R.P.B., SILVA, et al., (2019). SEAM is a single-degree-of-freedom modal analysis used to determine the loss factor and stiffness of the device.

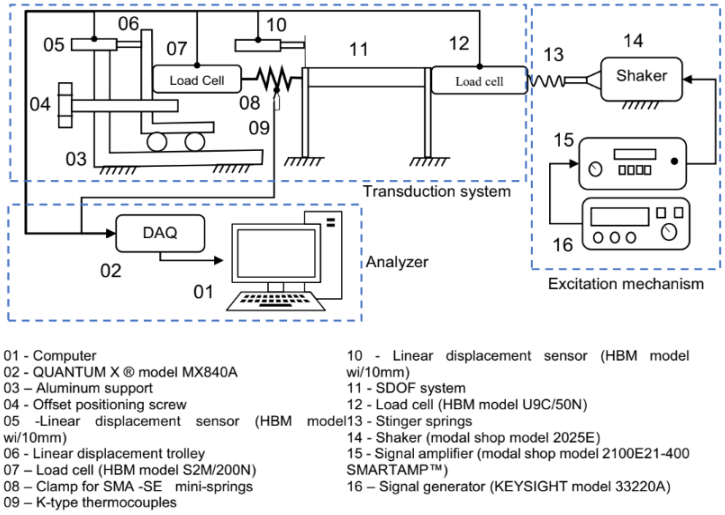

01 - Computer
02 - QUANTUM X ® model MX840A
03 – Aluminum support
04 - Offset positioning screw
05 -Linear displacement sensor (HBM model wi/10mm)
06 - Linear displacement trolley
07 – Load cell (HBM model S2M/200N)
08 – Clamp for SMA -SE mini-springs
09 – K-type thermocouples
10 - Linear displacement sensor (HBM model wi/10mm)
11 - SDOF system
12 - Load cell (HBM model U9C/50N)
13 - Stinger springs
14 - Shaker (modal shop model 2025E)
15 - Signal amplifier (modal shop model 2100E21-400 SMARTAMP™)
16 – Signal generator (KEYSIGHT model 33220A)

Figure 6 - SEAM. Source: Adapted from DOS REIS, R.P.B., SILVA, et al., (2019).

1. The blade (7) is fixed to the structure (6).
2. The carriage (10) is moved by the screw (12) until the load cell (9) makes contact with the blade (7). This position is set as the origin of the LVDT (11).
3. The load cell values (5, 9) are zeroed.
4. The screw (12) is displaced until the LVDT (11) reaches a displacement of 2 mm, which is the pre-displacement value in the test.
5. The flexible rod (4) is compressed and coupled to the structure (6) in such a way that the load cell (5) reaches 4 N.
6. The generator (1) generates a harmonic sine signal with a linear variation from 1 to 50 Hz over 300 s, which is amplified (2) and sent to the shaker (3).
7. The load cell (5) and LVDT (8) results are acquired using the Catman Data Acquisition (DAQ) software at a rate of 2400 Hz.
8. The process is repeated four times to ensure test repeatability and generate the average of the curves.

3 RESULTS

3.1 Characterization of transformation temperatures

Figure 7 depicts the RET curves obtained from the blade before and after forming, respectively, and Table 1 presents a comparison with the results obtained by Almeida (2020).

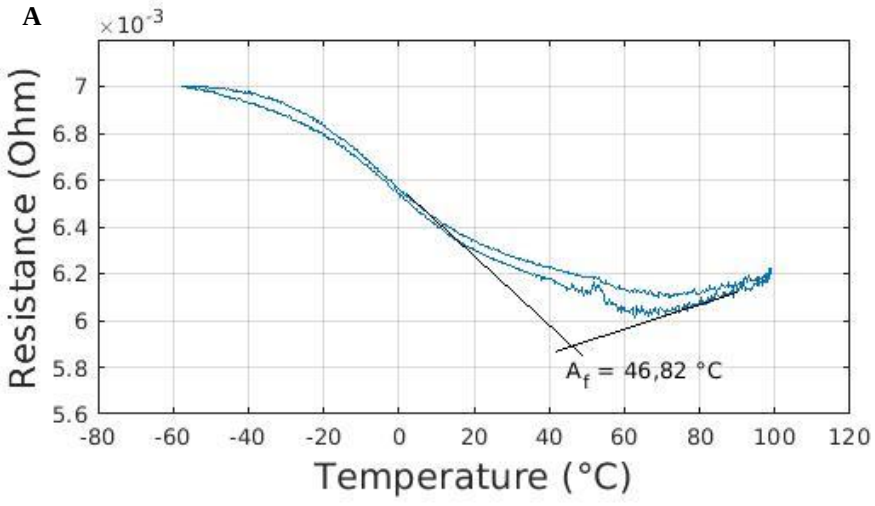

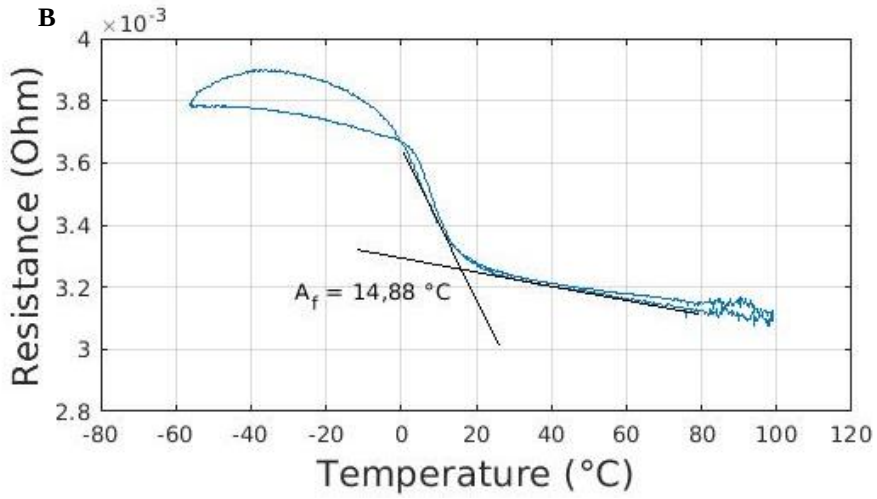

Figure 7. RET of Sample 1 - A) sheet, B) after fabrication. Source: Prepared by the author.

Table 1 - Comparison of RET results. Source: Prepared by the author.

	Manufactured spring	**Almeida (2020)**
Temperature Af before fabrication	46,82 °C	23, 57 °C
Temperature Af after fabrication	14,88 °C	14,10 °C

In this experiment, an Af temperature of 46.82 °C was obtained before shape setting, which is above the local ambient temperature (approximately 22 °C), indicating that the material is not fully in the austenitic phase. However, after the shape setting process, the Af temperature was reduced to 14.88 °C (Figure 7B). Therefore, the material tends to be fully in the austenitic phase at room temperature in order to take advantage of the superelasticity effect. This result was expected and is consistent with the studies by MOTEMANI (2009), which demonstrate that the final austenitic temperature decreases as the cooling rate increases. This result was similar to those obtained by Almeida (2020), since the same type of spring was manufactured.

3.2. Mechanical Characterization of NiTi LMF Sheets

Figure 8 shows the stress-strain curve obtained from the tensile test.

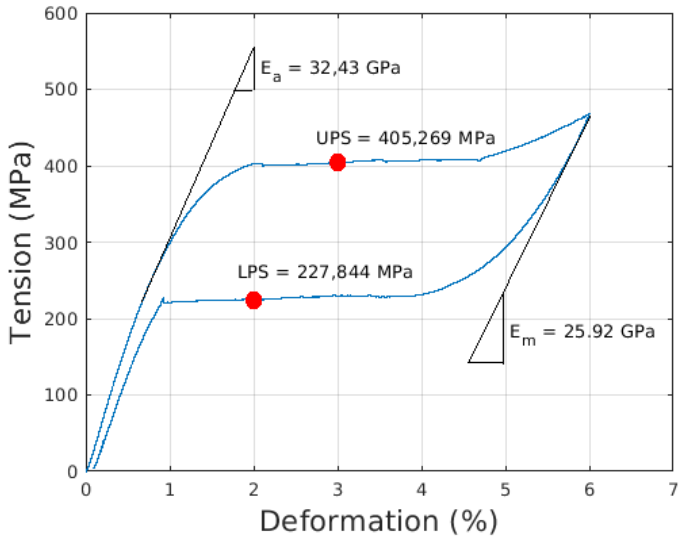

Figure 8. Tensile Test. Source: Prepared by the author.

Table 2 - Comparison between the results of the tensile test. Source: Prepared by the author.

	Manufactured spring	**Almeida (2020)**
Ea (GPa)	32,43	55,13
Em (GPa)	25,92	29,39
UPS (MPa)	405,269	434,600
LPS (MPa)	227,844	205,240
Elr (%)	0,0944	0,1790
σrup (MPa)	1285,230	638,220

The Young's modulus obtained from the tensile test was higher in the austenitic phase than in the martensitic phase, which was expected since the stiffness of the austenitic phase is about four times higher than that of the martensitic phase. These results were relatively lower compared to those obtained by ALMEIDA (2020), who had a higher stiffness index, making the material susceptible to failure at low load levels. The ultimate tensile strength was 1285.229 MPa, which was expected due to the natural convection cooling, similar to the method used by SENKO et al. (2022), who obtained an ultimate tensile strength of around 1200 MPa.

The difference between the plateau stresses (UPS and LPS) indicates approximately 44% of the UPS value, representing a high hysteresis area and therefore demonstrating a high damping potential, a value similar to that of Almeida (2020), who obtained a value of 50%. The residual elongation of the sample was 0.0944%, indicating that only a few cycles are needed to reach the stabilization of the elastic behavior.

3.3. Material Damping

Using the SEAM, the Nyquist diagram and Frequency Response Function (FRF) graphs of the spring were obtained for a pre-load of 1.5 mm to determine the hysteresis damping. Figure 9A shows the comparison between the system without the proposed spring and the system with the spring, while Figure 9B represents the amplitude of the system. It can be observed that the Nyquist circle of the system with the spring is reduced, indicating the high damping potential of the device. The hysteresis damping of the system without the spring is 0.276, whereas with the spring, this value increased to 1.283, resulting in a 78.44% increase. In the FRF (Figure 8B), a reduction of 15.092 dB in the system's amplitude can be observed when compared to the system without it.

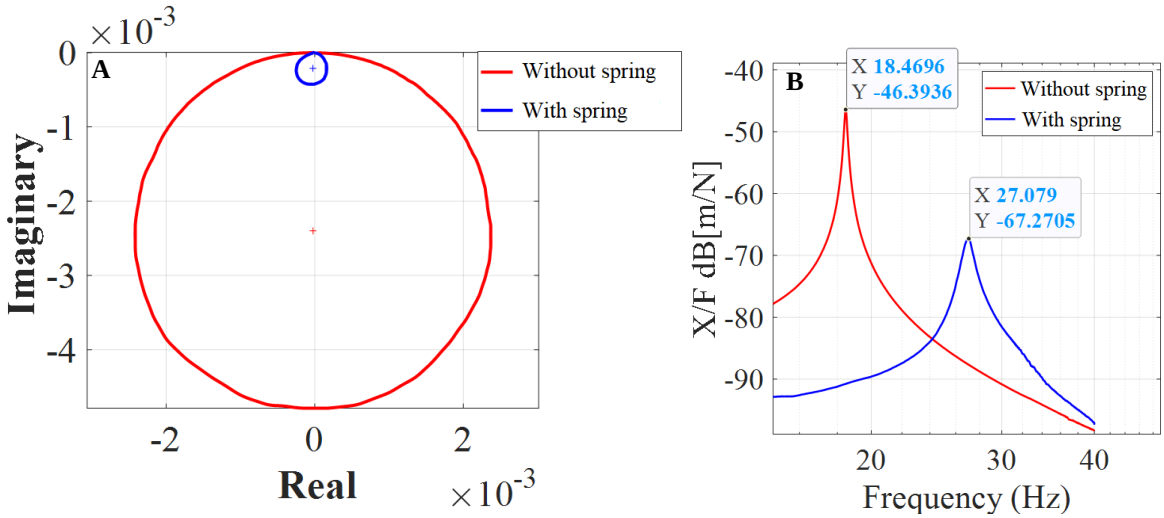

Figure 9. A) Nyquist Plot; B) FRF. Source: Prepared by the author.

The manufactured spring has a loss factor (η) of 14.78%, while Almeida's (2020) was 7.55%. The difference was expected, as reported by MOTEMANI (2009), who stated that samples with higher cooling rates tend to have a reduced loss factor.

4 CONCLUSION

In this research, experiments and studies were conducted on the application of heat treatment (HT) to obtain complex-shaped LMF-SE springs. Although the LMF-SE blade, after being treated, obtained a relatively high Af temperature, after shape setting, the temperature was below ambient, which is considered ideal. This observation is consistent with Almeida (2020).

Through the tensile test, it was possible to analyze that the material exhibits stable elastic behavior. The rupture stress was also determined, and it was found to be twice as high as that of Almeida (2020). The higher mechanical strength of the spring in this research overcomes the limitation observed in Almeida's study, where the low mechanical strength hindered the application of their springs in the rotating system.

Finally, the results obtained from the SEAM indicate that the manufactured spring has a higher hysteresis damping capacity, a reduction in the system's amplitude, and a higher loss factor compared to the results obtained by Almeida (2020).

Thus, the spring presented in this research demonstrates ideal properties for its application in rotating systems and proves to be advantageous compared to Almeida (2020), as it can be applied in the rotating system without premature fracture.

5 REFERENCES

ALMEIDA, V. S. Desenvolvimento e Testes de Atenuação de Vibrações em Mancal de Sistema Rotativo Aplicando Atuadores do Tipo Lâmina de Liga com Memória de Forma no Regime Superelástico. 2020 (Dissertação de Mestrado). Unidade Acadêmica de Engenharia Mecânica, Universidade Federal de Campina Grande.

DOS REIS, Rômulo Pierre Batista. Development of an equipment for thermal characterization of shape memory alloy actuators using thermoelectric effect. 2010. 58 f. Federal University of Campina Grande, 2010.

DOS REIS, Rômulo Pierre Batista. Efeito da incorporação de minimolas NiTi superelásticas no amortecimento estrutural: aplicações em atenuação passiva de pás de aero gerador. 2018. 123 f. UFCG, 2018.

GANDHI, M. V., THOMPSON, B. S. Smart Materials and Structures. [S.l.], Chapman & Hall, 1992.

PATOOR, E., LAGOUDAS, D. C., ENTCHEV, P. B., et al. "Shape memory alloys, Part I: General properties and modeling of single crystals", Mechanics of Materials, v. 38, n. 5–6, p. 391–429, maio 2006. DOI: 10.1016/j.mechmat.2005.05.027. Disponível em: https://linkinghub.elsevier.com/retrieve/pii/S0167663605001195.

SENKO, R. Passive attenuation of a rotating system using superelastic blades of SMA. 2018. 177 f. Federal University of Paraíba, 2018. DOI: https://repositorio.ufpb.br/jspui/handle/123456789/12967. Disponível em: https://repositorio.ufpb.br/jspui/handle/123456789/12967.

Senko R, Almeida VS, Dos Reis RPB, Oliveira AG, Silva AA, Rodrigues MC, de Carvalho LH, Lima AGB. Passive Attenuation of Mechanical Vibrations with a Superelastic SMA Bending Springs: An Experimental Investigation. Sensors (Basel). 2022 Apr 21;22(9):3195. doi: 10.3390/s22093195. PMID: 35590893; PMCID: PMC9103138.

SOUZA, E. F. De. Experimental Study of the Thermal and Dynamic Behavior of a Belleville Spring with NiTi Shape Memory Alloy. 2015. 26 f. Federal University of Campina Grande, 2015.

HEIDARI, B., KADKHODAEI, M., BARATI, M., et al. "Fabrication and modeling of shape memory alloy springs", Smart Materials and Structures, v. 25, n. 12, 10 nov. 2016. DOI: 10.1088/0964-1726/25/12/125003.

RAO, A., SRINIVASA, A. R., REDDY, J. N. Design of Shape Memory Alloy (SMA) Actuators. Cham, Springer International Publishing, 2015. Disponível em: http://link.springer.com/10.1007/978-3-319-03188-0. (SpringerBriefs in Applied Sciences and Technology).

MOTEMANI, Y., NILI-AHMADABADI, M., TAN, M. J., et al. "Effect of cooling rate on the phase transformation behavior and mechanical properties of Ni-rich NiTi shape memory alloy", Journal of Alloys and Compounds, v. 469, n. 1–2, p. 164–168, fev. 2009. DOI: 10.1016/j.jallcom.2008.01.153. Disponível em: https://linkinghub.elsevier.com/retrieve/pii/S0925838808002120.